Conductivity of solvated electrons in hexane investigated with terahertz time-domain spectroscopy

Ernst Knoesel[a)]
Department of Physics and Astronomy, Rowan University, Glassboro, New Jersey 08028

Mischa Bonn[b)]
Leiden Institute of Chemistry, P.O. Box 9502, 2300 RA Leiden, The Netherlands

Jie Shan
Department of Physics, Case Western Reserve University, Cleveland, Ohio 44106

Feng Wang and Tony F. Heinz[c)]
Departments of Physics and Electrical Engineering, Columbia University, New York, New York 10027

(Received 19 January 2004; accepted 8 April 2004)

We present investigations of the transient photoconductivity and recombination dynamics of quasifree electrons in liquid *n*-hexane and cyclohexane performed using terahertz time-domain spectroscopy (THz-TDS). Quasifree electrons are generated by two-photon photoionization of the liquid using a femtosecond ultraviolet pulse, and the resulting changes in the complex conductivity are probed by a THz electromagnetic pulse at a variable delay. The detection of time-domain wave forms of the THz electric field permits the direct determination of both the real and the imaginary part of the conductivity of the electrons over a wide frequency range. The change in conductivity can be described by the Drude model, thus yielding the quasifree electron density and scattering time. The electron density is found to decay on a time scale of a few hundred picoseconds, which becomes shorter with increasing excitation density. The dynamics can be described by a model that assumes nongeminate recombination between electrons and positive ions. In addition, a strong dependence of the quasifree electron density on temperature is observed, in agreement with a two-state model in which the electron may exist in either a quasifree or a bound state. © *2004 American Institute of Physics.* [DOI: 10.1063/1.1757442]

I. INTRODUCTION

In recent years terahertz time-domain spectroscopy (THz-TDS) (Ref. 1) has been successfully applied to investigate the frequency-dependent complex conductivity of a wide variety of material systems. Through such measurements, THz-TDS provides a noninvasive way to access microscopic transport properties, such as free-electron densities and scattering times. Furthermore, the exceptional time resolution afforded by the technique in a pump-probe scheme[2–36] has permitted the study of transient phenomena, including charge transport in systems out of equilibrium. In addition, for the case of liquids, THz-TDS has been used to obtain valuable information on intermolecular forces through analysis of the spectral features of the unexcited sample.[37–45] Here, following our initial report,[27] we employ THz-TDS to investigate transient photoconductivity in the nonpolar liquids of hexane and cyclohexane.

The nature of solvated electrons in nonpolar liquids such as hexane has been widely studied, motivated both by the intrinsic interest of the problem and by applications to the detection of ionizing radiation.[46–50] Early radiolysis and (time-resolved) photoionization experiments were largely concerned with the pathways and efficiency of the generation process of the excess electrons,[51–54] the mechanism of charge transport,[55–58] and the electron-ion recombination process.[59–67] Later experiments examined the variation of the electron mobility with temperature,[53,68] pressure,[57,68–72] and molecular geometry,[48,56] the connection between electron mobility and free-ion yield,[51,53,54] and recombination rates of electrons with electron scavengers.[59,73–75]

From these studies, possible pathways and typical time scales for photogenerated electrons have emerged. They are illustrated in Fig. 1. Following generation, the electron loses its excess translational energy within a few picoseconds during the thermalization phase. A key parameter in this process is the ion–electron separation distance after thermalization. This quantity depends on the kinetic energy of the electron, but is typically on the order of 4–6 nm for hexane.[47,66,76,77] Another important length scale in the problem is the Onsager radius, a quantity defined as the distance at which the thermal diffusive forces acting on the electron balance the Coulomb attraction of the ion. It is given by

$$r_{\mathrm{ons}} = e^2/(4\pi\varepsilon_r\varepsilon_0 k_B T), \tag{1}$$

with ε_r and ε_0 denoting, respectively, the relative and vacuum permittivity.[78] The Onsager radius is a measure of the ion–electron separation beyond which a thermalized electron is likely to escape from the Coulomb attraction of its

[a)]Electronic mail: knoesel@rowan.edu
[b)]Current affiliation: FOM-Institute for Atomic and Molecular Physics, Kruislaan 407, 1098 SJ Amsterdam, The Netherlands.
[c)]Electronic mail: tony.heinz@columbia.edu

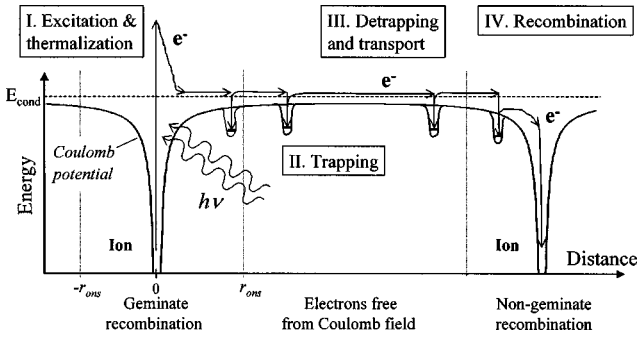

FIG. 1. Schematic representation of dynamics of photogenerated electrons in hexane. After the initial ionization process, an electron may either recombine (geminately) with its parent ion or escape from the corresponding Coulomb attraction. An electron that escapes from its parent ion will eventually reach another positive ion, so that nongeminate recombination can occur. The solvated electrons exist in both trapped and quasifree states, the ratio of populations varying with the trap depth and the temperature. The motion of the quasifree electrons is characterized by a mean scattering time γ_0.

parent ion. For *n*-hexane, $r_{\mathrm{ons}}=30$ nm. It has been observed that during the first 10 ps, roughly 70% of photoexcited electrons in *n*-hexane will recombine with their respective parent ions.[63,66] Geminate recombination is a nonexponential process, and therefore a fraction of the remaining electrons will continue to be recaptured over a much longer time scale.[52,67,79] After diffusing outside the Onsager radius, an electron may escape from its parent ion and move through the liquid. In a photoexcited bulk liquid, these electrons ultimately recombine nongeminately.

The observation of a sharp increase with temperature of the conductivity of liquids containing equivalent densities of solvated electrons led to the development of the two-state model.[53,74] In this picture, most electrons are trapped in bound states that are essentially immobile and do not contribute appreciably to charge transport. They may, however, be thermally excited into a highly mobile quasifree state, which leads to significant conductivity of the ionized liquid. The density of quasifree electrons, generally assumed to be in thermal equilibrium with the bound electrons, depends strongly on the temperature and on the well depth of the bound states. The latter reflects the molecular geometry and structure of the liquid. It is estimated to lie in the range of 100–200 meV for linear-chain alkanes.[80] In liquids with highly mobile electrons, Hall measurements have enabled a direct evaluation of the quasifree electron mobility.[81–83]

Transient absorption spectroscopy has provided detailed information on the lifetime of electrons in liquids.[60–64,66,67,84] It has, however, provided less insight into the *transport characteristics* of these charge carriers, a property that is not manifested directly in the optical spectra. Radiolysis experiments, on the other hand, only provide data on the dc conductivity.[53,57,79] This quantity may be difficult to interpret in terms of the fundamental scattering times in the system, given the complication inherent in measuring the *average* response of electrons in a two-state system. In addition, excited electrons with short lifetimes may be difficult to observe in radiolysis experiments. THz-TDS offers a useful complement to these two types of existing probes of electrons in liquids. As will be shown below, the response of ionized nonpolar liquids at the THz frequencies can be attributed to the conductivity of the quasifree electrons. Measurements in this frequency range then allow their density and scattering time to be determined. THz-TDS is also well suited for dynamical studies, permitting the lifetime of photogenerated mobile charge carriers to be measured.

In this paper, which expands upon our initial report,[27] we provide new data and a detailed analysis of electron conductivity and electron lifetime dynamics in *n*-hexane and cyclohexane. After outlining our experimental procedures (Sec. II), we present the experimental results (Sec. III). We then turn (Sec. IV) to an analysis of the THz wave forms in differential measurements, focusing in particular on the relative contributions to the THz signal from transmission and reflection losses of the THz beam as it traverses the sample. In the discussion (Sec. V), the Drude model is introduced (Sec. V B) and it is demonstrated how electron densities and scattering times can be obtained. Using this analysis, we then discuss the results of the temperature-dependent conductivity measurements (Sec. V C) and the different activation energies observed for the photoinduced conductivity of *n*-hexane and cyclohexane. Measurements at various pump fluences reveal only a weak dependence of the scattering rate on the number of excited electrons, indicating that electron–electron and electron–ion interactions are relatively unimportant for scattering of the quasifree electrons. The electron–ion recombination process, which occurs on a slower time scale, however, depends strongly on the excitation density. We show (Sec. V D) that the corresponding experimental data can be understood in terms of a nongeminate recombination mechanism.

II. EXPERIMENT

The apparatus employed for THz-TDS is shown schematically in Fig. 2. The laser source for these measurements was a regeneratively amplified, mode-locked Ti:sapphire system. It provided pulses of 150 fs duration at a central wavelength of 810 nm with an energy of 1 mJ/pulse and a repetition rate of 1 kHz. Pulsed THz radiation was produced by optical rectification of these laser pulses in a 1-mm-thick ZnTe crystal.[85] This approach yielded appreciable intensity from 0.1 to 2 THz. The resulting THz beam was collimated and focused on the sample to a spot diameter below 1 mm. The electric field of the THz radiation was detected after passing through the sample by electro-optic detection in a second ZnTe crystal.[86,87]

The samples, *n*-hexane and cyclohexane (spectroscopic grade, Alpha Aesar), were probed in the form of a free-standing liquid jet, with a thickness varying from 30 to 100 μm, depending on nozzle type. Alternatively, we employed a liquid flow cell with a sample thickness varying from 300 to 1000 μm. The cell was made of two water-free fused silica windows of 2.1 mm thickness. The use of two sample geometries permitted us to access a wide range of carrier densities in the experiments. For the jet, with its short optical path length, we probed relatively high excitation densities. For the sample cell, with its longer optical path length, significantly lower excitation densities could be probed; its use at high excitation densities was, however, constrained by two-

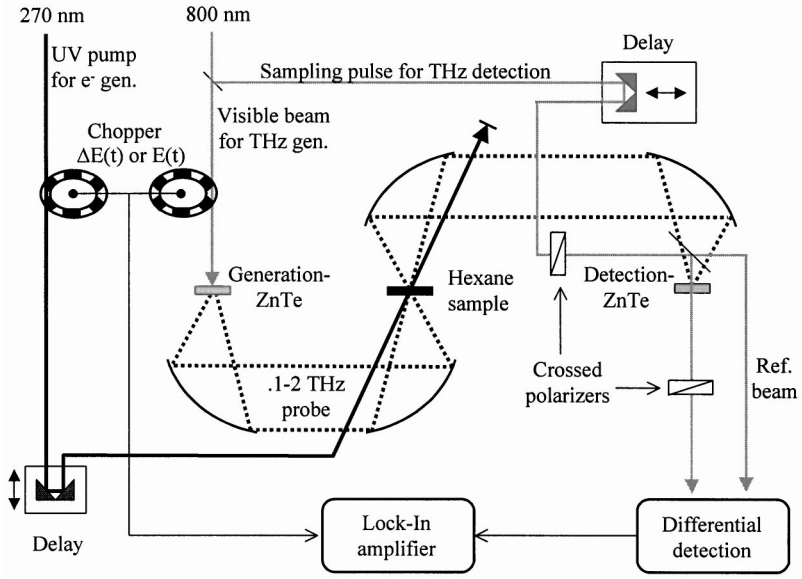

FIG. 2. The experimental setup for THz time-domain spectroscopy with a UV pump for photoionization of the liquid sample. THz radiation is generated and detected in ZnTe crystals. After generation, paraboloidal mirrors are used to collimate and focus the THz onto the hexane sample. By inserting a chopper into the visible beam for generation, we can record the transmitted THz wave form by lock-in detection. Alternatively, by chopping the UV excitation beam and detecting the induced modulation in the transmitted THz wave form, we can measure the THz response of the solvated electrons.

photon absorption in the windows of the cell. We experimentally determined the relevant sample thickness l by comparing the group velocities of the THz beam in air and in the sample[88–90] and making use of the known THz refractive index of hexane. For both sample configurations, a flow speed of at least 2 m/s was employed to assure fresh liquid for each laser shot. The temperature of the liquid was adjusted by heating/cooling the liquid reservoir. Temperature variation caused by optical pumping was found to be negligible.

The solvated electrons in the hexane samples were generated through a two-photon ionization process by 270-nm ultraviolet (UV) pulses. Two such photons provide an energy of 9.18 eV, which exceeds the ionization potential of both *n*-hexane [$I_{\text{ion}}=8.6\,\text{eV}$ (Ref. 91)] and cyclohexane [$I_{\text{ion}}=8.44\,\text{eV}$ (Ref. 92)]. The UV pulses were created by frequency tripling 90% of the 810-nm laser radiation in a sequence of two β-barium borate (BBO) crystals. The resulting UV radiation, with a pulse energy of 50 μJ, was directed to the sample surface at a 15° angle of incidence. The UV excitation was aligned using an aperture for maximal overlap with the THz probe beam.

An important experimental issue concerns maintaining sufficiently homogeneous photoexcitation of the liquid. In an ideal measurement, this would be achieved simply by making the UV pump beam size far greater than that of the THz probe beam. In practice, however, this is not necessarily easy to achieve. On the one hand, one needs to maintain a sufficiently high UV pump fluence to drive the two-photon ionization process in the sample, despite the limited UV pump energy of $\sim$50 μJ pulse. This implies a maximum pump spot size for a desired excitation density. On the other hand, one is limited by the rather large focal diameter of the THz probe beam associated with the long wavelength of the radiation. The consequence of spatial variation of the excitation density over the THz probe volume is not restricted to the obvious measurement of the average properties of a sample with differing local electron densities. Rather, one must consider spectral distortions of the THz response that might be introduced by diffraction of the THz beam in propagating through the spatially inhomogeneous sample. Possible THz wave form distortion may be further enhanced because the spectral content of the THz probe generally varies across the transverse profile of the beam. These THz diffraction effects have been extensively investigated by Bromage *et al.*[93] and Nahata and Heinz[94] for the extreme case of conducting apertures of various sizes. The studies demonstrate the possibility of significant changes in the THz wave form as a result of diffraction. In an attempt to quantify these effects in our experiments, we varied the spot size of the excitation beam and introduced controlled diffraction by placing metal apertures in the focal plane of the THz beam. The measurements suggest that under our experimental conditions, diffraction effects had little influence on the THz signal within the frequency range of interest (0.4–1.5 THz). We do not attempt to interpret data at lower frequencies, however, where the effects of diffraction are expected to be more pronounced. In some of the investigations, our interest did not lie in the frequency dependence of the induced conductivity $\Delta\sigma(\omega)$, but rather in the magnitude of $\Delta\sigma$ as a measure of the density of quasifree electrons. For these studies diffraction effects were relatively unimportant, and the UV pump beam was sometimes focused within the THz probe spot to permit us to achieve a higher density of photogenerated carriers.

We have performed three distinct types of measurements with our experimental apparatus. In the first, we detect the THz electric field $E(t)$ that propagates through air and through our sample (with the UV pump beam blocked). A comparison of the two wave forms provides the THz conductivity of the unexcited sample. In this measurement, the transmitted THz wave form is recorded by varying the delay of the femtosecond optical sampling pulse (see Fig. 3).

In the second type of measurement, we determine the pump-induced changes in the THz wave form, $\Delta E(t;\tau_d)$, at a specified UV-pump/THz-probe delay time of τ_d. These measurements yield the change in the THz conductivity associated with ionization of the hexane sample. We detect the weak induced modulation of the THz signal from photoexci-

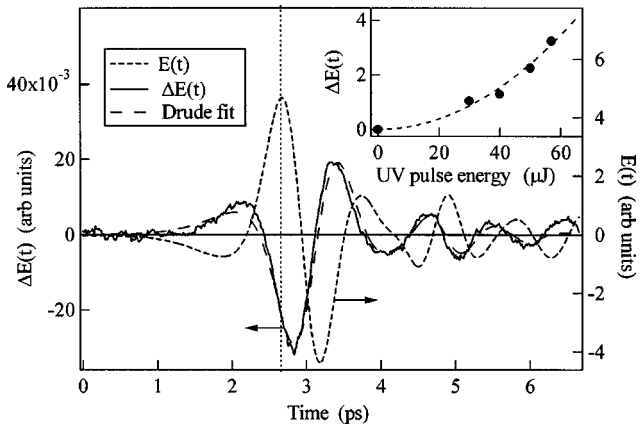

FIG. 3. THz wave form after transmission through the *n*-hexane jet $E_{\mathrm{out}}^{\mathrm{hex}}(t)$ together with the UV-pump-induced changes of this wave form, $\Delta E(t;\tau_d)$, at a UV-pump/THz-probe delay of $\tau_d = 70$ ps. The pump-induced changes are on the order of 1% in magnitude and of opposite sign compared to the THz wave form. The inset shows the quadratic dependence of the THz ΔE signal on fluence of the UV excitation pulse, as expected for a two-photon ionization process.

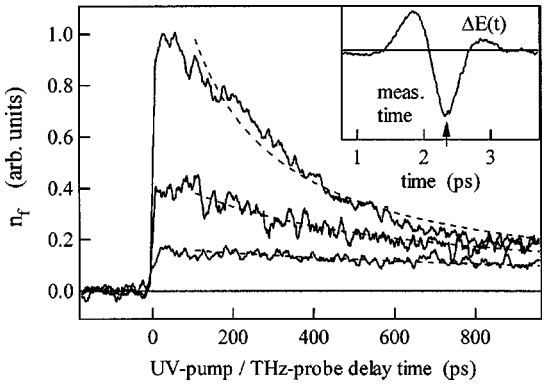

FIG. 4. Dependence of the THz signal strength ΔE on the UV-pump/THz-probe delay time τ_d for an *n*-hexane sample with photoexcitation at three different pump fluences. As discussed in the text, ΔE is proportional to the quasifree electron density n_f. The strength of the THz signal ΔE was recorded at the maximum of $\Delta E(t)$ (see inset). The fluence dependent decay rates are typical of a nongeminate recombination process. The results of the model described in the text are shown as dashed lines.

tation using chopping of the UV-pump beam and lock-in detection of the THz wave form. Since the THz pulse itself has a temporal width of ~1 ps, such measurements can only be interpreted as a time-varying conductivity when the properties of the sample do not change significantly on the corresponding time scale.[95] For the measurements presented here, this requirement is fulfilled.

In a third scheme, we capture the temporal evolution of the sample following photoexcitation. This is accomplished by recording the amplitude of changes in the THz field $\Delta E(t_{\max};\tau_d)$, as a function of the delay between THz-probe and UV-pump pulses τ_d. The THz response is measured at a sampling time $t_{\max}$, where the maximal modulation of the THz field is observed. As in the previous arrangement, the UV-pump beam is chopped and the change in the THz field is detected with lock-in techniques. In these measurements, the time dependence of the UV-pump-induced modulation is determined by scanning of the pump/probe delay time τ_d. For a straightforward interpretation of such measurements, one must confirm that the THz wave form $\Delta E(t)$ does not change appreciably with τ_d.

III. RESULTS

Figure 3 depicts the THz electric field $E(t)$ passing through the hexane jet. Also shown is the THz wave form for the pump-induced change in the THz wave form $\Delta E(t;\tau_d)$ at a pump/probe delay of $\tau_d = 70$ ps. The pump-induced change is on the order of 1% of the THz field. It is of opposite sign compared to the transmitted THz wave form, corresponding to a pump-induced absorption. In addition, the shift of $\Delta E(t;\tau_d)$ compared to $E(t)$ indicates a pump-induced decrease in the THz refractive index. The inset in the figure displays the quadratic variation of the magnitude of ΔE on the fluence of the UV pump pulse, as may be expected for a two-photon ionization process.

The dependence of the induced change in the THz wave form $\Delta E(t;\tau_d)$ on the pump/probe delay time τ_d was also examined. We found that there was no significant difference in the wave form as a function of τ_d. We were then able to record temporal evolution of the *amplitude* of the induced change as a function of delay simply by scanning τ_d with the femtosecond optical sampling pulse for the THz wave form measurement fixed at the maximum of $\Delta E(t)$, as indicated in the inset of Fig. 4. If the wave form is unaltered, the magnitude of the THz signal ΔE is directly proportional to the quasifree electron density n_f, as will be discussed below in more detail. The results of such experiments for three different excitation densities are depicted in the main panel of Fig. 4. The decay occurs on a ~300-ps time scale for the highest excitation densities, but slows down considerably when the energy in the UV pulse is reduced. Measurements in cyclohexane (not shown) yielded similar behavior.

We have also examined the induced THz response $\Delta E(t;\tau_d)$ as a function of the temperature of the sample. Again, the shape of the THz wave forms was essentially unchanged. On the other hand, the induced change in the amplitude of the THz wave form ΔE, proportional to the quasifree electron density n_f, showed a strong dependence on temperature. The results for a pump-probe delay time of $\tau_d = 70$ ps are summarized in Fig. 5. The data are presented as an Arrhenius plot of the logarithm of n_f versus the reciprocal temperature. They show a higher apparent activation energy of 300 meV for cyclohexane compared with a value of 165 meV for *n*-hexane.

IV. ANALYSIS OF THz WAVE FORMS

In this section, we describe how we determined the THz material response of the sample (with and without photoexcitation) from the measured wave forms. The key feature in this treatment is the inclusion of the effects of the multiple reflections, arising from the two boundaries of the sample. For the photoexcited sample, the analysis is carried out in the limit of a weak perturbation to the THz response, as is appropriate for our experimental conditions. Here we describe the response of the sample to the THz radiation in terms of a

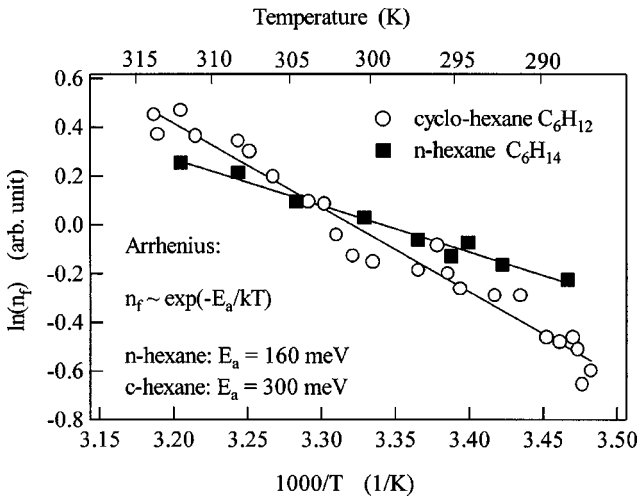

FIG. 5. Temperature dependence of the quasifree electron density n_f for *n*-hexane and cyclohexane, shown as an Arrhenius plot. The relative quasifree electron densities for each liquid were determined from the strength of the induced THz response ΔE at a UV-pump/THz-probe delay of 70 ps. Different apparent activation energies, as indicated in the graph, are observed for the two liquids.

(complex) refractive index. This formulation is, of course, fully equivalent to one involving a complex dielectric function or a complex conductivity to describe the material response.

In order to extract the THz refractive index from the measurements, we first compare the THz electric field measured with ($E_{\text{out}}^{\text{hex}}$) and without ($E_{\text{out}}^{\text{air}}$) the sample. Figure 6 illustrates schematically the transmission of a THz pulse through the sample. A THz pulse with electric field E_{in} enters a sample of thickness l at an angle of incidence of θ. The sample has a (complex THz) refractive index n_2 and is surrounded by a medium with refractive index n_1. At the first interface, the THz pulse experiences a transmission factor t_{12} (associated with a reflection coefficient of r_{12}). It then propagates through the sample and undergoes a change in amplitude by the complex factor p_2. The pulse leaves through the second interface with an additional transmission factor of t_{21}. In addition, multiple reflections at the interfaces contrib-

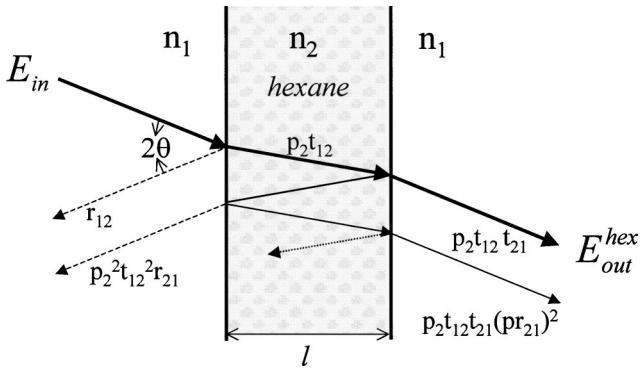

FIG. 6. Schematic illustration of the transmission of a THz pulse through the sample. The THz radiation enters from a medium with a refractive index of n_1 into the sample of thickness l and refraction index n_2. The resultant THz electric field, denoted by $E_{\text{out}}^{\text{hex}}$, is related to the incident field E_{in} through the Fresnel factors described in the text.

ute to the emerging THz electric field, especially for the case of large refractive index mismatches. The resultant transmitted THz field, denoted by $E_{\text{out}}^{\text{hex}}$, is given by

$$E_{\text{out}}^{\text{hex}}(\omega)=\frac{p_2 t_{12} t_{21}}{1-(p_2 r_{21})^2}E_{\text{in}}(\omega), \tag{2}$$

where we have written the formula in the frequency domain as a function of angular frequency ω. The denominator of the equation accounts for the effect of multiple reflections. In the derivation of this formula, the contributions to $E_{\text{out}}^{\text{hex}}$ from multiple reflections are assumed to overlap *spatially* and to add together coherently. For the case of normal incidence, the Fresnel coefficients and the propagation factor simplify to the well-known expressions

$$t_{12}t_{21}=\frac{4n_1n_2}{(n_1+n_2)^2}, \quad r_{21}=\frac{n_1-n_2}{n_1+n_2},$$
$$\text{and} \quad p_2=\exp\left(\frac{\text{in}_2\omega l}{c}\right). \tag{3}$$

From a second measurement of the THz electric field *without* the sample, we determine the wave form $E_{\text{out}}^{\text{air}}$. This wave form obeys the same propagation condition as $E_{\text{out}}^{\text{hex}}$ in Eq. (2), but with the refractive index of hexane substituted for that of air. Using the known THz refractive index of hexane of $n=1.42$,[96] we may obtain the sample thickness l from a comparison of the measured THz wave forms $E_{\text{out}}^{\text{hex}}$ and $E_{\text{out}}^{\text{air}}$.

Our main focus, however, lies not on the response of the unexcited liquid, but on the extraction of the pump-induced changes in the sample's complex conductivity or, equivalently, in its complex refractive index Δn_2. The transmitted THz electric field with the pump beam switched on, $E_{\text{out}}^{\text{hex}}+\Delta E_{\text{out}}^{\text{hex}}$, is determined by the refractive index of the sample of $n_2+\Delta n_2$, according to

$$E_{\text{out}}^{\text{hex}}(\omega)+\Delta E_{\text{out}}^{\text{hex}}(\omega)=\frac{p_2^+ t_{12}^+ t_{21}^+}{1-(p_2^+ r_{21}^+)^2}E_{\text{in}}(\omega), \tag{4}$$

with the Fresnel coefficients t_{12}^+, t_{21}^+, r_{21}^+, and the propagation factor p_2^+ representing the behavior of the *photoexcited* liquid. The changes in the THz wave form, $\Delta E_{\text{out}}^{\text{hex}}$, are at most a few percent (see Fig. 3), which indicates that we are operating in the regime of weak perturbation. The Fresnel relations for normal incidence can be linearized for small changes to yield

$$\frac{t_{12}^+ t_{21}^+}{t_{12}t_{21}}=1-\Delta n_2\frac{n_2-n_1}{n_2(n_2+n_1)}; \quad \frac{r_{21}^+}{r_{21}}=1$$
$$+\Delta n_2\frac{2n_1}{n_2^2-n_1^2}; \quad \frac{p_2^+}{p_2}=1+\Delta n_2\frac{i\omega l}{c}. \tag{5}$$

Equations (2), (4), (5) then lead to the following expression for the change in the refractive index:

$$\Delta n_2=\left[\frac{i\omega l}{c}-\frac{n_2-n_1}{n_2(n_2+n_1)}+MR\right]^{-1}\frac{\Delta E_{\text{out}}^{\text{hex}}(\omega)}{E_{\text{out}}^{\text{hex}}(\omega)}. \tag{6a}$$

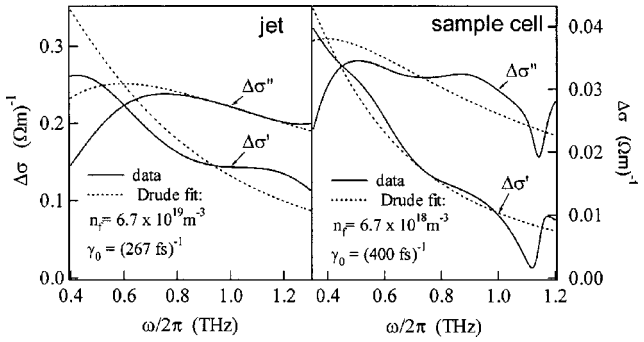

FIG. 7. Photoinduced change in THz complex conductivity, $\Delta\sigma=\Delta\sigma'+i\Delta\sigma''$, as a function of frequency $\omega/2\pi$ for *n*-hexane in two different sample arrangements, a jet and a flow cell (solid lines). A fit to the Drude model (dotted lines) is also shown. The experimental traces were obtained from the data in Fig. 3 using Eqs. (6) and (7). The frequency dependence of $\Delta\sigma$ is similar for the two cases, even though the magnitude varies by a factor of 10.

This equation shows that the transmitted field is affected by the pump-induced changes in the refractive index through (i) modification of the propagation through the sample (first term), (ii) changes in reflective losses at the two interfaces (second term), and (iii) the contribution from multiple reflections (third term, denoted as MR) of

$$\mathrm{MR}=\frac{2(p_2 r_{21})^2}{1-(p_2 r_{21})^2}\left(\frac{i\omega l}{c}-\frac{2n_1}{n_2^2-n_1^2}\right). \tag{6b}$$

For thicker samples, such as our sample cell, the propagation term dominates the sum in Eq. (6a). The interface and the multiple reflection terms can then be omitted. For thin samples, however, as for the liquid jet, the full expression must be used to correctly extract Δn_2 from the measured $E_{\mathrm{out}}^{\mathrm{hex}}(t)$ and $\Delta E_{\mathrm{out}}^{\mathrm{hex}}(t)$ wave forms. Note that in contrast to a nonpertubative treatment of the induced changes in the sample's THz response, the inversion process from the THz wave forms to the THz material response remains straightforward, since all of the parameters in Eq. (6) are defined by the unexcited properties of the materials. For the jet, we interpret n_1 as the refractive index of air ($n_1=1$). For the sample cell, the surrounding material is the fused silica window of the cell with $n_1=1.95$.[97]

In what follows, we will demonstrate that the changes in complex refractive index are attributable to the motion of quasifree electrons in photoexcited hexane. It is therefore more suitable to discuss the results in terms of an induced change in the complex conductivity. For $|\Delta n|\ll 1$, the relation between these two quantities reads

$$\Delta\sigma(\omega)=-2i\omega\varepsilon_0 n_2\Delta n. \tag{7}$$

V. INTERPRETATION AND DISCUSSION

A. Quasifree electrons as the source of the signal

Figure 7 shows the photoinduced changes in conductivity, $\Delta\sigma(\omega)=\Delta\sigma'(\omega)+i\Delta\sigma''(\omega)$, as a function of the THz frequency $\omega/2\pi$ in *n*-hexane. Data are presented for both the jet and the flow-cell arrangement. The calculated traces were obtained using Eq. (6), after having performed Fourier transforms of the experimental time-domain THz wave forms like those of Fig. 3. The results were then formulated as an induced change in the complex conductivity, rather than in the refractive index, by means of Eq. (7). The frequency dependence of the real and imaginary part of $\Delta\sigma$ is similar for measurements in both the liquid jet and sample cell. The UV pump pulse can be seen to create an increase in the real conductivity ($\Delta\sigma'>0$) in the hexane sample. The imaginary part ($\Delta\sigma''>0$) is also positive and of the same order of magnitude as the real part.

We now consider the origin of these pump-induced changes in the THz response of the liquid. They can arise in principle from all species generated or modified by the UV pump: ions, excited neutral molecules, and electrons in both the bound and quasifree state. The observed quadratic dependence of the signal on the excitation energy indicates a two-photon excitation process (see inset Fig. 3) associated with the production of ions and electrons. Further, the addition of the electron scavenger CCl_4 to the *n*-hexane liquid leads to a rapid quenching of the THz response as a function of the pump-probe delay time. Since the number of ions would not decrease in the presence of the electron scavenging molecules, we conclude that electrons are the predominant source of the signal.[66] This result is just as we would expect: The quasifree electrons with their low effective mass interact strongly with THz radiation.[1,2] One must, however, also consider the bound electrons. Although these electrons are expected to exhibit a much weaker response to THz radiation than the quasifree electrons, they are present at much higher density (see Sec. V C). Simple estimates suggest that the contribution of bound and quasifree electrons to the THz response, after accounting for their different populations, may be comparable. In the experiment, however, photoexcitation produces an increase in both the real and imaginary parts of the conductivity. Bound electrons would only influence significantly the imaginary part of the conductivity, and would lead to a contribution of negative sign. We thus conclude that the dominant contribution to the observed THz signal arises from the quasifree electrons. In addition, the temperature-dependent measurements show an exponential increase of the real and imaginary part of the conductivity, as expected within the two-state model for a signal arising from the quasifree electrons. We cannot, however, rule out the possibility of a weak contribution from bound electrons.

B. Drude model

Having identified the quasifree electrons as the source of our pump-induced change in the THz response, we would like to describe the frequency-dependent conductivity within the framework of a suitable transport model. For that purpose we adopt the simple Drude picture.[98] In this approximation, the complex conductivity is given by

$$\Delta\sigma(\omega)=\frac{i\varepsilon_0\omega_p^2}{\omega+i\gamma_0}. \tag{8}$$

Here γ_0 defines the scattering rate. This parameter characterizes the motion of the electron and is important for both the electron conductivity and diffusivity. The quantity ω_p

$=\sqrt{e^2 n_f/(\varepsilon_0 m^*)}$ is the plasma frequency of the quasifree electrons, which are assumed to have an effective mass m^* and a density n_f. In the expression of Eq. (8) we see that the *frequency dependence* of $\Delta\sigma$ is determined solely by the scattering rate γ_0, whereas the plasma frequency ω_p (which scales with the quasifree electron density) affects only the *amplitude* of the response.

The dotted lines in Fig. 7 show the Drude fit to the experimental data. The agreement between data and model is adequate for both the jet (left panel) and the flow cell (right panel). For frequencies below 0.4 THz, the THz wavelength becomes comparable to the limited spot size of the UV pump beam (~1 mm). An interpretation below this frequency has not been attempted, since diffraction effects might strongly influence our observation. We attribute the residual departures from the Drude model to this effect, as well as to the experimental uncertainty in recording the THz wave forms. It should be noted that the influence of noise appears much greater in the Fourier transformed data than in fitting the THz wave form directly in the time domain, as illustrated in Fig. 3.

The inferred scattering times, $\tau=\gamma_0^{-1}$, are 270 fs for the jet, and 400 fs for the flow cell. The possible significance of this difference will be discussed below. The analysis of several experiments yields a preferred scattering time of 310 $\pm$100 fs. It has been argued that the quasifree electron mobility for *cyclohexane* should exceed that of *n*-hexane because of the more spherical nature of the former molecule.[56,68] In fact, we find that the observed scattering rates for *n*-hexane and cyclohexane are indistinguishable within experimental accuracy. Within the Drude model, the scattering rate γ_0 can be related to the dc mobility of the quasifree electrons μ_f by the expression $\mu_f=e/(m^*\gamma_0)$. Assuming that the quasifree electron mass m^* is given by the electron rest mass m_e, we obtain a value of μ_f $=560\,\mathrm{cm^2\,V^{-1}\,s^{-1}}$ from our experimental scattering rate.

It is instructive to compare the quasifree electron mobility derived from THz-TDS with the (average) drift mobilities obtained from radiolysis measurements. In radiolysis, the information available is the total density of solvated electrons and the dc conductivity with its temporal evolution. From these experimental data one can obtain the average properties of the solvated electrons and hence the average mobility μ_D. Since most of the solvated electrons are in bound states that do not contribute substantially to charge transport, the average mobility of the solvated electrons is far lower than that of the quasifree electrons. Radiolysis measurements have reported an *average* electron mobility of μ_D $=0.074-0.09\,\mathrm{cm^2\,V^{-1}\,s^{-1}}$ for electrons in *n*-hexane (and $\mu_D=0.28-0.4\,\mathrm{cm^2\,V^{-1}\,s^{-1}}$ for cyclohexane).[50,53,54,79] Assuming a negligible contribution to the mobility from bound electrons, the ratio of the electron mobility for a quasifree electron (μ_f) to that of an average electron mobility (μ_D) will just be given by the corresponding ratio of densities, i.e., $\mu_f/\mu_D=n_t/n_f$, where n_t is the total density of solvated electrons. Since the vast majority of the electrons reside in bound states, we can also write this ratio as $n_t/n_f\approx n_b/n_f$ $\equiv R$, where n_b is the density of bound electrons.

Using the experimental value of μ_D $=0.074-0.09\,\mathrm{cm^2\,V^{-1}\,s^{-1}}$ for the average mobility and our experimentally derived $\mu_f=560\,\mathrm{cm^2\,V^{-1}\,s^{-1}}$ for the quasifree electrons, we obtain $R=6200-7500$. In the analysis of the radiolysis measurements, the temperature dependence of the effective mobility has been used to estimate the ratio R $=n_b/n_f$ of the densities of bound to quasifree electrons in the two-state model. This value, however, depends critically on the model of the liquid structure and the nature of quasifree electron transport (ballistic or diffusive), as well as on the density of trap sites. Values of R ranging from 400 to 5200 have been reported in the literature.[53,55,99] Our derived value of R is comparable to, but slightly greater than the published estimates. One may ask whether a dependence of the ratio R on the density of solvated electrons is to be expected. Clearly at sufficiently high densities one might envisage saturation of the traps associated with the bound states. This regime, however, would appear to require extremely high electron densities of $\sim 10^{25}\,\mathrm{m^{-3}}$ (see Ref. 100), well in excess of those reached in these studies.

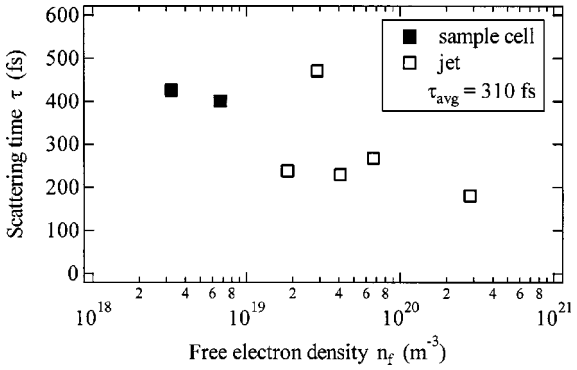

FIG. 8. Scattering time, $\tau=1/\gamma_0$, of the quasifree electrons as a function of their density n_f. Note that although n_f varies by almost two orders of magnitude ($4\times10^{18}-2.5\times10^{20}\,\mathrm{m^{-3}}$), the scattering time remains relatively constant, with an average value of (310$\pm$100) fs.

In the quasiballistic model of electron transport,[101,102] almost every scattering event leads to trapping of a quasifree electron. Within this picture, our experimentally derived scattering time of 310 fs can then be interpreted as the lifetime of the electron in the quasifree state. By way of comparison, a time scale of a few hundred femtoseconds has been observed for a transition from a quasifree to a localized electron state in solid alkane films.[103] In the framework of a dynamic equilibrium the bound–to–free electron ratio R also reflects the ratio of the lifetimes within the respective states. From the minimum lifetime of ~310 fs in the quasifree state we may infer a lifetime of the electron in the trap state on the order of 100's of picoseconds.

Figure 8 summarizes the results for the scattering time $\tau=\gamma_0^{-1}$ of quasifree electrons in *n*-hexane as a function of the excitation density. The excitation density has been converted into a density of quasifree electrons using the Drude analysis. These values also agree well with estimates based on the experimental excitation density, the ionization cross section and losses associated with geminate recombination. The variation of the quasifree electron density for different measurements spans almost two orders of magnitude ($4\times10^{18}-2.5\times10^{20}\,\mathrm{m^{-3}}$). This variation, however, does not

significantly affect the scattering time of the quasifree electrons, which averages to (310 ± 100) fs. These results indicate that for the electron densities in this study, scattering events of the quasifree electron with other electrons or with ions are not of great significance. The possible trend towards shorter scattering times with increasing electron density may be caused by experimental factors related to the size of the UV-pump spot, which must be focused more and more tightly to achieve higher electron densities. This situation may enhance the diffraction effects mentioned above and precludes drawing any definite conclusions from the weak trend in the density dependence of the scattering time in Fig. 8.

C. Temperature dependence of the signal

As mentioned above, no significant change in the form of the photoinduced THz response of the liquids was observed as a function of temperature over the relatively limited range of temperatures investigated (280–315 K). We did, however, see a significant change in amplitude. Within the Drude model (or any other model with noninteracting charge carriers), we can interpret the change in the THz response as linearly proportional to the density of quasifree electrons n_f. Figure 5 shows that this density can be modeled as increasing with temperature in an activated manner. For *n*-hexane, the apparent activation energy is 160 meV; for cyclohexane, it is 300 meV. It is tempting to relate the apparent activation energies directly to energy differences between the bound and the free state. Such an analysis would be appropriate if our conditions implied a constant total density of solvated electrons n_t for each measurement. In fact, however, what is maintained constant is the UV pump fluence for the photoionization process. For this situation, several additional factors need to be considered, as we now discuss.

The temperature dependence of the density of quasifree electrons n_f can, generally speaking, be influenced by several distinct processes for conditions of constant photoexcitation. These include: (i) the temperature dependence of the efficiency of creation of a thermalized electron–ion pair following the photoexcitation, (ii) the temperature dependence of the geminate recombination probability, and (iii) the temperature dependence of the ratio of bound to quasifree electrons.

With respect to (i), the creation efficiency of an electron–ion pair depends on the two-photon absorption cross section. As discussed by Holroyd and Russell,[104] this quantity is expected to be essentially temperature independent. Thus we do not anticipate that this factor will contribute significantly to the observed temperature dependence of the electron density over the limited range of temperatures examined experimentally.

Regarding factor (ii), the separation probability, as described by the Onsager model,[78] is strongly temperature dependent because of the variation of the Onsager radius r_{ons} with temperature [see Eq. (1)]. Indeed for low escape probabilities, the model leads to an *exponential* increase in the density of escaping electrons with temperature. This dependence has been verified experimentally by measuring the free-ion yield in radiolysis experiments[51] and the dc conductivity of photoionized tetramethyl-*p*-phenylenediamine (TMPD) in *n*-hexane.[104] It should be noted that these experiments detect electrons microseconds after generation when all geminate recombination has already been completed. The temperature dependence of the free-ion yield is associated with the electrons that are initially positioned near the boundary of the Onsager sphere and for which their ultimate fate as either geminately recombining electrons or escaping electrons takes a relatively long time to unfold.[47] In our experiments, however, we typically measure the electron density 70 ps after photoionization. On this time scale, the *rapid* component of the geminate recombination process has already occurred. The possible geminate recombination of electrons initially located at greater distances may not yet have reached completion. Thus the sharpness of the temperature dependence associated with geminate recombination for the THz measurements may be reduced compared with the corresponding effect in traditional radiolysis measurements. It is, however, still expected to be significant.

Factor (iii) is considered to be the dominant source of the temperature dependence of the average mobility observed in radiolysis measurements. Within the two-state model of immobile trapped electrons and mobile quasifree electrons, this effect arises from the increasing population of the quasifree electrons with increasing sample temperature. Using a model of the electrons bound with an energy e_0 in traps of density n_t, Mozumder[105] has proposed the following expression for the ratio of quasifree to bound electrons:

$$R^{-1}=n_t^{-1}(2\pi mk_BT/h^2)^{3/2}e^{-e_0/k_BT}. \tag{9}$$

The binding energy e_0 is related to the experimentally accessible activation energy E_a by $e_0=0.885\,E_a$ (Ref. 100). At room temperature, the ratio R^{-1} is dominated by the exponential term, which originates from the thermally activated detrapping process. Temperature-dependent radiolysis measurements of the average mobility report an exponential temperature dependence, with an effective activation energy $E_a=180$ meV for *n*-hexane and $E_a=150$ meV for cyclohexane at 300 K.[68] The lower activation energy for cyclohexane agrees well with theoretical predictions.[55] It also results in a higher density of quasifree electrons and thus a higher average mobility for cyclohexane, as observed experimentally: $\mu_D=0.28-0.4\,\mathrm{cm^2\,V^{-1}\,s^{-1}}$ for cyclohexane[54] and $\mu_D=0.074-0.09\,\mathrm{cm^2\,V^{-1}\,s^{-1}}$ for *n*-hexane.[56]

As we have just indicated, the role of thermal generation of quasifree electrons from trap states [factor (iii)] can account for much of the observed temperature dependence in the quasifree electron density inferred from our THz measurements. Indeed, in the case of *n*-hexane, our experimental activation energy of 160 meV essentially replicates the value observed for the activation energy in the radiolysis measurements, which was attributed to this source. For cyclohexane, however, the THz measurements give an apparent activation energy of 300 meV, while the corresponding radiolysis measurements yield an activation energy of just 150 meV. This difference may be attributed to the temperature dependence of the probability of geminate carrier recapture [factor (ii) above]. What remains unclear, however, is why this factor would be much more significant for cyclohexane than for

n-hexane. One possible answer lies in the motion of ions, which is significant in cyclohexane compared to *n*-hexane.[106]

D. Electron-ion recombination dynamics

In the past, electron-ion recombination processes have been primarily investigated using transient optical absorption techniques, with wavelengths ranging from the visible to the mid-IR.[62–64,66] In contrast to THz spectroscopy, these methods are also potentially sensitive to bound electrons, ions and excited molecules, and therefore their focus has been on the initial recombination process between excited electrons and photogenerated ions. In order to link our results with such earlier investigations, we also recorded a transient absorption signal using an 810-nm probe beam. We observed a decay on the time scale of 3 ps to one third of the initial signal, in good agreement with earlier reports in the literature.[66] Since this decay rate was found to be independent of the excitation density, the underlying process responsible for this decay was identified as a *geminate* recombination between the excited electron and its parent ion.

In contrast, in the THz experiment, as illustrated in Fig. 4, we do not see evidence of such a rapid decay. The reason for the absence of this feature is unclear. It can, however, be explained, at least in part, by the reduced time resolution of the THz measurement compared with that of the optical probe. While the rapid decay component is not seen in the THz measurements, we can observe a slower decay over 100's of ps. Unlike the early-time behavior observed with the optical pulse, this rate exhibits a marked dependence on the excitation density. We interpret the increased decay rate of the quasifree electron density with increased excitation as the consequence of the presence of a higher density of ions. It is thus a signature of a *nongeminate* recombination process, although a small contribution from geminate recombining electrons to the THz signal might still be present.

The analysis of the time-resolved experiments is facilitated by the observation from Eqs. (6)–(8) that the observed $\Delta E(t)$ signal is directly proportional to the quasifree electron density n_f. Furthermore, assuming equilibration between electrons in the quasifree and the bound states, we can interpret $\Delta E(t)$ as proportional to the total density of solvated electrons n_t. The key aspect of the nongeminate recombination process is the dependence of the rate on the product of the density of the solvated electrons and the density of the ions. As a simple model of the decay dynamics after an initial rapid phase of geminate recombination, we introduce a second-order rate law for the evolution of the solvated electron density:[107]

$$\dot{n}_t(t) = -kn_t^2(t). \tag{10}$$

Here $n_t(t)$ is the time-dependent total electron density and k the rate constant; we have replaced the product of the ion and electron densities that one would expect on the right-hand side of Eq. (10) with the square of the solvated electron density using conservation of charge. The solution of this differential equation leads to

$$\frac{n_t(t)}{n_t(0)} = \frac{1}{1+kn_t(0)t}, \tag{11}$$

with $n_t(0)$ denoting the initial solvated electron density. This equation illustrates a key characteristic of nongeminate recombination, namely that the decay rate depends critically on the initial density $n_t(0)$. This simple model is seen to be capable of reproducing the data of Fig. 4 adequately. As is physically appropriate, we have used the same value of k but distinct value $n_t(0)$ for the different initial excitation densities. Although the model of Eq. (11) was introduced in a heuristic manner, it has also been derived for charge transport governed by diffusion and a Coulomb attraction between the two species.[107] The rate constant k is then related to the sum of the mobility of the two species μ by

$$k = \frac{e}{\varepsilon_0 \varepsilon_r}\mu. \tag{12}$$

The sum of the mobilities is dominated by the electron mobility. Considering all of the solvated (bound and quasifree) electrons, the relevant mobility has a value of $\mu_D = 0.074-0.09\,\mathrm{cm^2\,V^{-1}\,s^{-1}}$ for *n*-hexane.[50,56] By using this value and Eqs. (11) and (12), we are able to calculate the initial total density of electrons as $n_t(0) = 3.3-4\times10^{22}\,\mathrm{m^{-3}}$ for the experiment at the highest excitation densities (see Fig. 4). This value is compatible with the estimated total electron density based on the quasifree electron density derived from the fit to the Drude model.

VI. CONCLUSION

In this paper we have applied the method of THz time-domain spectroscopy to probe transport in photoexcited liquids, namely, *n*-hexane and cyclohexane. The method provides measurement capabilities that complement established transport and optical characterization techniques. The THz technique provides direct information on the frequency-dependent conductivity of the material and its temporal evolution following photoexcitation. As we have seen, this information can provide valuable insight into the fundamental aspects of the charge transport process.

In our experiments, we found that the THz response arises predominantly from the motion of the photoexcited quasifree electrons. From the frequency dependence of the conductivity and application of the Drude model, we were able to extract a scattering time of 310 ± 100 fs for quasifree electron densities in the range of $10^{18}-10^{20}\,\mathrm{m^{-3}}$, depending on the conditions of the photoexcitation process. The corresponding mobility of the quasifree electrons was found to be dramatically larger than the previously determined *average* electron mobility. A high value for the free-electron mobility had, however, already been predicted by the two-state model of solvated electrons. In this picture, only a small fraction of the solvated electrons, the quasifree ones, contribute to the mobility, with the majority of the electrons remaining in essentially immobile trapped states. The ratio of the free-electron mobility to the average electron mobility reflects the ratio of the concentration of bound to quasifree electrons. With the approximation of dynamic equilibrium, this factor also corresponds to the ratio of the lifetime in the bound state to that in the free state. Since the lifetime of the quasifree electrons cannot fall below our experimentally determined

scattering time of 310 ± 100 fs, we infer residence times of electrons in the bound state as long as hundreds of picoseconds.

Experiments were performed to examine the influence of the temperature of the liquid on charge transport properties. Over the somewhat limited range of available temperatures, no change in carrier scattering rate was observed from our analysis of the measured frequency-dependent conductivity. For identical photoexcitation conditions, however, the density of quasifree electrons was found to change strongly with temperature and could be described as a thermally activated process. Since we expect nearly the same initial density of electrons irrespective of the temperature, one may readily explain this activated behavior in terms of the role of temperature in producing thermally excited quasifree electrons. Such an analysis suggests that the inferred activation energy should correspond to the energy needed to produce a quasifree electron from a bound electron. While this picture was compatible with the results for the binding energy of trap states in *n*-hexane, the apparent activation energy for cyclohexane differed from the previous determination of the binding energy. This discrepancy probably reflects the temperature dependence of the geminate recombination probability.

The THz probe was also used to follow the recombination dynamics through the temporal evolution of the quasifree electron density. A time scale of $\sim$1 ns was observed for the decay of this density, with a rate depending strongly on the initial electron/ion density created by the photoexcitation process. We thus concluded that the observed recombination process is predominantly *nongeminate* in character, at least for the time scale of our measurements. Modeling the recombination process assuming diffusive electron motion, we were able to reproduce the nonexponential temporal shape of the decay curve for different initial electron densities. An interesting aspect of this part of the study is the absence of a THz signature of the electrons undergoing geminate recombination, a feature that should be significant at early delay times of a few picoseconds. This observation, which stands in sharp contrast to behavior seen with femtosecond optical probe pulses, could simply reflect the influence of the reduced time resolution of the THz measurement. It is, however, difficult to understand the degree of suppression of this response solely in these terms. A different factor might be a decreased mobility of those electrons in the immediate proximity of their parent ions that are subject to rapid geminate recombination. Further examination of the THz response at short delay times following photoexcitation and a detailed comparison of these findings with the results of optical probing remains an interesting direction for future investigations.

ACKNOWLEDGMENTS

The authors gratefully acknowledge partial support for this work from the MRSEC Program of the National Science Foundation under Award No. DMR-0213574 and U.S. Department of Energy, Office of Basic Energy Sciences, through the Catalysis Science Program. Work by one of the authors (J. S.) was supported at Case Western Reserve University under NSF grant DMR-0349201.

[1] M. C. Beard, G. M. Turner, and C. A. Schmuttenmaer, J. Phys. Chem. B **106**, 7146 (2002).
[2] E. Hendry, F. Wang, J. Shan, T. F. Heinz, and M. Bonn, Phys. Rev. B **69**, 081101 (2004).
[3] V. K. Thorsmolle, R. D. Averitt, X. Chi, D. J. Hilton, D. L. Smith, A. P. Ramirez, and A. J. Taylor, J. Chem. Phys. **120**, 4755 (2004).
[4] D. Turchinovich, P. U. Jepsen, B. S. Monozon, M. Koch, S. Lahmann, U. Rossow, and A. Hangleiter, Phys. Rev. B **68**, 241307 (2003).
[5] J. Demsar, R. D. Averitt, and A. J. Taylor, J. Supercond. **17**, 143 (2004).
[6] A. Leitenstorfer, R. Huber, F. Tauser, and A. Brodschelm, Phys. Status Solidi B **238**, 455 (2003).
[7] F. Kadlec, C. Kadlec, P. Kuzel, P. Slavicek, and P. Jungwirth, J. Chem. Phys. **120**, 912 (2004).
[8] J. Demsar, R. D. Averitt, A. J. Taylor, W. N. Kang, H. J. Kim, E. M. Choi, and S. I. Lee, Int. J. Mod. Phys. B **17**, 3675 (2003).
[9] J. Shan, F. Wang, E. Knoesel, M. Bonn, and T. F. Heinz, Phys. Rev. Lett. **90**, 247401 (2003).
[10] R. A. Kaindl, M. A. Carnahan, D. Hagele, R. Lovenich, and D. S. Chemla, Nature (London) **423**, 734 (2003).
[11] G. A. Khodaparast, D. C. Larrabee, J. Kono, D. S. King, J. Kato, T. Slupinski, A. Oiwa, H. Munekata, G. D. Sanders, and C. J. Stanton, J. Appl. Phys. **93**, 8286 (2003).
[12] S. P. Jamison, J. L. Shen, D. R. Jones, R. C. Isaac, B. Ersfeld, D. Clark, and D. A. Jaroszynski, J. Appl. Phys. **93**, 4334 (2003).
[13] R. Huber, F. Tauser, A. Brodshelm, and A. Leitensdorfer, Phys. Status Solidi B **234**, 207 (2002).
[14] F. A. Hegmann, R. R. Tykwinski, K. P. H. Lui, J. E. Bullock, and J. E. Anthony, Phys. Rev. Lett. **89**, 227403 (2002).
[15] G. M. Turner, M. C. Beard, and C. A. Schmuttenmaer, J. Phys. Chem. B **106**, 11716 (2002).
[16] M. C. Beard, G. M. Turner, and C. A. Schmuttenmaer, Nano Lett. **2**, 983 (2002).
[17] M. Schall and P. U. Jepsen, Appl. Phys. Lett. **80**, 4771 (2002).
[18] A. Leitensdorfer, R. Huber, F. Tauser, A. Brodschelm, M. Bichler, and G. Abstreiter, Physica B **314**, 248 (2002).
[19] M. C. Beard, G. M. Turner, and C. A. Schmuttenmaer, J. Phys. Chem. A **106**, 878 (2002).
[20] M. C. Beard, G. M. Turner, and C. A. Schmuttenmaer, J. Appl. Phys. **90**, 5915 (2001).
[21] M. C. Beard, G. M. Turner, and C. A. Schmuttenmaer, J. Phys. Chem. B **106**, 7146 (2002).
[22] H. Wald, P. Seidel, and M. Tonouchi, Physica C **362**, 324 (2001).
[23] C. Messner, H. Kostner, R. A. Hopfel, and K. Unterrainer, J. Opt. Soc. Am. B **18**, 1369 (2001).
[24] P. U. Jepsen, W. Schairer, I. H. Libon, U. Lemmer, N. E. Hecker, M. Birkholz, K. Lips, and M. Schall, Appl. Phys. Lett. **79**, 1291 (2001).
[25] R. D. Averitt, A. I. Lobad, C. Kwon, S. A. Trugman, V. K. Thorsmolle, and A. J. Taylor, Phys. Rev. Lett. **87**, 017 401 (2001).
[26] K. P. H. Lui and F. A. Hegmann, Appl. Phys. Lett. **78**, 3478 (2001).
[27] E. Knoesel, M. Bonn, J. Shan, and T. F. Heinz, Phys. Rev. Lett. **86**, 340 (2001).
[28] M. Schall and P. U. Jepsen, Opt. Lett. **25**, 13 (2000).
[29] R. D. Averitt, G. Rodriguez, J. L. W. Siders, S. A. Trugman, and A. J. Taylor, J. Opt. Soc. Am. B **17**, 327 (2000).
[30] D. J. Cook, J. X. Chen, A. A. Morlino, and R. M. Hochstrasser, Chem. Phys. Lett. **309**, 221 (1999).
[31] R. McElroy and K. Wynne, Phys. Rev. Lett. **79**, 3078 (1997).
[32] S. S. Prabhu, S. E. Ralph, M. R. Melloch, and E. S. Harmon, Appl. Phys. Lett. **70**, 2419 (1997).
[33] G. Haran, W. D. Sun, K. Wynne, and R. M. Hochstrasser, Chem. Phys. Lett. **274**, 365 (1997).
[34] R. H. M. Groeneveld and D. Grischkowsky, J. Opt. Soc. Am. B **11**, 2502 (1994).
[35] B. I. Greene, J. F. Federici, D. R. Dykaar, A. F. J. Levi, and L. Pfeiffer, Opt. Lett. **16**, 48 (1991).
[36] M. C. Nuss, D. H. Auston, and F. Capasso, Phys. Rev. Lett. **58**, 2355 (1987).
[37] P. Mounaix, M. Moustakim, S. Le Boiteux, J. P. Delville, R. Wunenburger, and L. Sarger, Appl. Phys. Lett. **83**, 5095 (2003).
[38] M. R. Kutteruf, C. M. Brown, L. K. Iwaki, M. B. Cambell, T. M. Korter, and E. J. Heiweil, Chem. Phys. Lett. **375**, 337 (2003).
[39] B. L. Yu, F. Zeng, Q. Xing, and R. R. Alfano, Appl. Phys. Lett. **82**, 4633 (2003).

[40] M. L. T. Asaki, A. Redondo, T. A. Zawodzinski, and A. J. Taylor, J. Chem. Phys. **116**, 8469 (2002).
[41] D. S. Venables and C. A. Schmuttenmaer, J. Chem. Phys. **113**, 11 222 (2000).
[42] C. Ronne, K. Jensby, B. J. Loughnane, J. Fourkas, O. F. Nielsen, and S. R. Keiding, J. Chem. Phys. **113**, 3749 (2000).
[43] B. N. Flanders, X. M. Shang, N. F. Scherer, and D. Grischkowsky, J. Phys. Chem. A **103**, 10 054 (1999).
[44] C. Ronne, L. Thrane, P. O. Astrand, A. Wallquist, K. V. Mikkelsen, and S. R. Keiding, J. Chem. Phys. **107**, 5319 (1997).
[45] D. M. Mittleman, M. C. Nuss, and V. L. Colvin, Chem. Phys. Lett. **275**, 332 (1997).
[46] W. F. Schmidt, Nucl. Instrum. Methods Phys. Res. A **327**, 83 (1993).
[47] B. S. Yakovlev and L. V. Lukin, in *Photodissociation and Photoionization*, edited by K. P. Lawley (Wiley, New York, 1985), p. 99.
[48] R. A. Holroyd and W. F. Schmidt, Annu. Rev. Phys. Chem. **40**, 439 (1989).
[49] R. A. Holroyd, in *Radiation Chemistry*, edited by Farhataziz and M. A. J. Rodgers (VCH, New York, 1987).
[50] W. F. Schmidt, *Liquid State Electronics of Insulating Liquids* (CRC, Boca Raton, FL, 1997).
[51] W. F. Schmidt and A. O. Allen, J. Chem. Phys. **52**, 2345 (1970).
[52] M. Tachiya and W. F. Schmidt, J. Chem. Phys. **90**, 2471 (1988).
[53] N. Gee, C. Senanayake, and G. R. Freeman, J. Chem. Phys. **89**, 3710 (1988).
[54] J. P. Jay-Gerin, T. Goulet, and I. Billard, Can. J. Chem. **71**, 287 (1993).
[55] Y. A. Berlin, L. Nyikos, and R. Schiller, J. Chem. Phys. **69**, 2401 (1978).
[56] N. Gee and G. R. Freeman, J. Chem. Phys. **78**, 1951 (1983).
[57] R. C. Munoz, R. A. Holroyd, K. Itoh, K. Nakagawa, M. Nishikawa, and K. Fueki, J. Phys. Chem. **91**, 4639 (1987).
[58] A. Vertes, J. Chem. Phys. **79**, 5558 (1983).
[59] J. H. Baxendale, C. Bell, and P. Wardman, J. Chem. Soc., Faraday Trans. 1 **69**, 776 (1972).
[60] T. W. Scott and C. L. Braun, Can. J. Chem. **63**, 228 (1985).
[61] C. L. Braun and T. W. Scott, J. Phys. Chem. **91**, 4436 (1987).
[62] R. W. Bowman, H. Lu, and K. B. Eisenthal, J. Chem. Phys. **89**, 606 (1988).
[63] M. Sander, U. Brummund, K. Luther, and J. Troe, J. Phys. Chem. **97**, 8378 (1993).
[64] F. H. Long, H. Lu, and K. B. Eisenthal, J. Phys. Chem. **99**, 7436 (1995).
[65] F. F. Brazgun, V. A. Nadtchochenko, I. V. Rubtsov, and L. V. Lukin, Chem. Phys. **211**, 469 (1996).
[66] L. D. A. Siebbeles, U. Emmerichs, A. Hummel, and H. J. Bakker, J. Chem. Phys. **107**, 9339 (1997).
[67] A. Volkmer, K. Wynne, and D. J. S. Birch, Chem. Phys. Lett. **299**, 395 (1999).
[68] S. S.-S. Huang and G. R. Freeman, Can. J. Chem. **56**, 2388 (1978).
[69] R. C. Munoz, R. A. Holroyd, and M. Nishikawa, Phys. Chem. Liq. **14**, 2969 (1985).
[70] K. Itoh, M. Nishikawa, and R. A. Holroyd, J. Chem. Phys. **104**, 1545 (1996).
[71] K. Itoh, R. A. Holroyd, and M. Nishikawa, J. Phys. Chem. B **102**, 3147 (1998).
[72] R. A. Holroyd and M. Nishikawa, Radiat. Phys. Chem. **64**, 19 (2002).
[73] A. O. Allen and R. A. Holroyd, J. Phys. Chem. **78**, 796 (1974).
[74] A. O. Allen, T. E. Gangwer, and R. A. Holroyd, J. Phys. Chem. **79**, 25 (1975).
[75] A. Mozumder, J. Phys. Chem. **99**, 6557 (1995).
[76] L. V. Lukin and A. A. Balakin, Chem. Phys. **265**, 87 (2001).
[77] A. Mozumder, J. Phys. Chem. A **106**, 7062 (2002).
[78] L. Onsager, Phys. Rev. **54**, 554 (1938).
[79] J. M. Warman, in *The Study of Fast Processes and Transient Species by Electron Pulse Radiolysis*, edited by J. H. Baxendale and F. Busi (Reidel, Dordrecht, 1982), p. 520.
[80] N. Gee and G. R. Freeman, J. Chem. Phys. **86**, 5716 (1987).
[81] R. C. Munoz and G. Ascarelli, Phys. Rev. Lett. **51**, 215 (1983).
[82] K. Itoh, R. C. Munoz, and R. A. Holroyd, J. Chem. Phys. **90**, 1128 (1989).
[83] K. Itoh, R. A. Holroyd, and M. Nishikawa, J. Chem. Phys. **94**, 2073 (1991).
[84] A. Liu, Jr., M. C. Sauer, and A. D. Trifunac, J. Phys. Chem. **97**, 11 265 (1993).
[85] A. Nahata, A. Weling, and T. F. Heinz, Appl. Phys. Lett. **69**, 2321 (1996).
[86] A. Nahata, D. H. Auston, T. F. Heinz, and C. Wu, Appl. Phys. Lett. **68**, 150 (1996).
[87] Q. Wu and X. C. Zhang, Appl. Phys. Lett. **70**, 1784 (1997).
[88] D. Grischkowsky, S. R. Keiding, M. van Exter, and Ch. Fattinger, J. Opt. Soc. Am. B **7**, 2006 (1990).
[89] C. Ronne, P. O. Astrand, and S. R. Keiding, Phys. Rev. Lett. **82**, 2888 (1999).
[90] N. Katzenellenbogen and D. Grischkowsky, Appl. Phys. Lett. **61**, 840 (1992).
[91] J. Casanovas, R. Grob, D. Delacroix, J. P. Guelfucci, and D. Blanc, J. Chem. Phys. **75**, 4661 (1981).
[92] A. E. Ostafin and S. Lipsky, J. Chem. Phys. **98**, 5408 (1993).
[93] J. Bromage, S. Radic, G. P. Agrawal, C. R. Stroud, Jr., P. M. Fauchet, and R. Sobolewski, J. Opt. Soc. Am. B **15**, 1953 (1998).
[94] A. Nahata and T. F. Heinz, IEEE J. Quantum Electron. **2**, 701 (1996).
[95] M. C. Beard and C. A. Schmuttenmaer, J. Chem. Phys. **114**, 2903 (2001).
[96] J. E. Petersen and S. R. Kelding, IEEE J. Quantum Electron **10**, 2518 (1992).
[97] *American Institute of Physics Handbook*, 3rd ed. (McGraw-Hill, New York, 1982).
[98] M. P. Marder, *Condensed Matter Physics* (Wiley, New York, 2000).
[99] R. Schiller, S. Vass, and J. Mandices, Int. J. Radiat. Phys. Chem. **5**, 491 (1973).
[100] A. Mozumder, Chem. Phys. Lett. **233**, 167 (1995).
[101] J. C. Dyre and T. B. Schroder, Rev. Mod. Phys. **72**, 873 (2000).
[102] A. Mozumder, Res. Chem. Intermed. **25**, 243 (1999).
[103] N. H. Ge, C. M. Wong, R. L. Lingle, Jr., J. D. McNeill, K. J. Gaffney, and C. B. Harris, Science **279**, 202 (1998).
[104] R. A. Holroyd and R. L. Russell, J. Phys. Chem. **78**, 2128 (1974).
[105] A. Mozumder, Chem. Phys. Lett. **207**, 245 (1993).
[106] M. C. Sauer, I. A. Shkrob, J. Yan, K. Schmidt, and A. D. Trifunac, J. Phys. Chem. **100**, 11 325 (1996).
[107] A. Hummel, in *Radiation Chemistry*, edited by Farhataziz and M. A. J. Rodgers (VCH, New York, 1987).